Sound & Vibration 2025, 59(4), 3496.
doi: https://doi.org/10.59400/sv3496

Article

Fuzzy-grey relational optimization for active vibration control in smart composite beams: a multi-objective framework with experimental validation

Yogeesh N[1,2,*], Markala Karthik[1], N Raja[3], Asokan Vasudevan[4,5], Rashmi M[6], Ashalatha K S[7]

[1] Department of Electrical and Electronics Engineering, SR University, Warangal 506371, India
[2] Department of Mathematics, Government First Grade College, Tumkur 572101, India
[3] Department of Visual Communication, Sathyabama Institute of Science and Technology, Chennai 600119, India
[4] Faculty of Business and Communications, INTI International University, Nilai 71800, Malaysia
[5] Faculty of Business and Communications, Wekerle Business School, 1083 Budapest, Hungary
[6] Department of Computer Science, Government First Grade College, Bengaluru 560057, India
[7] Department of Mathematics, Vedavathi Government First Grade College, Hiriyur 577598, India
*** Corresponding author:** Yogeesh N, yogeesh.r@gmail.com

CITATION

N Yogeesh, Karthik M, Raja N et al. Fuzzy-grey relational optimization for active vibration control in smart composite beams: a multi-objective framework with experimental validation. Sound & Vibration. 2025; 59(4): 3496. https://doi.org/10.59400/sv3496

ARTICLE INFO

Received: 4 July 2025
Revised: 22 August 2025
Accepted: 24 August 2025
Available online: 31 August 2025

Abstract: This paper presents a hybrid fuzzy logic–grey relational analysis (Fuzzy–GRA) framework for multi-objective optimization of active vibration control (AVC) in smart composite beams. A fuzzy-adaptive Linear Quadratic Regulator (LQR) is developed, in which the LQR weighting matrices are adjusted online based on a grey relational grade that synthesizes vibration attenuation, control energy, and robustness metrics. A finite-element model incorporating piezoelectric actuator–sensor coupling is used to generate a hypothetical modal-test dataset, and both numerical simulations and laboratory experiments on an aluminium cantilever beam validate the method. Simulation results show up to 25 % and 13.6 % improvements in vibration attenuation over deterministic and genetic-algorithm-tuned LQR, respectively, while reducing control energy by 12.5 %. Experimental trials confirm 29.7 % and 14.3 % attenuation gains, 15.3 % energy savings, and a 41.7 % enhancement in robustness under ± 10 % parameter variations. Environmental robustness tests demonstrate only a 2.1 % performance drop under a 20 °C temperature increase, compared to an 8.1 % drop for conventional tuning. One-way ANOVA confirms that the observed improvements are highly significant ($F \gg F_{(2,12,0.05)}$). The proposed Fuzzy–GRA approach thus offers a mathematically rigorous yet practical strategy for tuning AVC gains under uncertainty, with promising applications in structural health monitoring and precision engineering.

Keywords: fuzzy logic; grey relational analysis (GRA); adaptive Linear Quadratic Regulator (adaptive LQR); multi-objective optimization; piezoelectric actuator-sensor; vibration attenuation; control energy efficiency

1. Introduction

1.1. Background on smart composite beams and active vibration control

Smart composite beams-typically glass- or carbon-fiber laminates with surface-bonded piezoelectric actuator-sensor patches have attracted intensive research for their ability to sense, process, and actively suppress unwanted vibrations in real time [1, 2]. Piezoelectric actuators convert electrical control signals into mechanical strain, counteracting structural oscillations; collocated sensors measure the residual response for feedback. Such active vibration control (AVC) schemes have been applied

in aerospace, precision machinery, and civil-structure health monitoring to improve fatigue life, reduce noise, and enhance dynamic stability [3].

The beam is clamped at the left end ($x = 0$) and free at the right end ($x = L$). Surface-bonded piezoelectric actuator (A) and sensor (S) patches are symmetrically placed along the beam's span. The actuator converts control voltage into mechanical strain to counteract vibrations, while the sensor measures structural response. Both top and side views are shown to clarify actuator/sensor positions, dimensions, and boundary constraints (see the **Figure 1**).

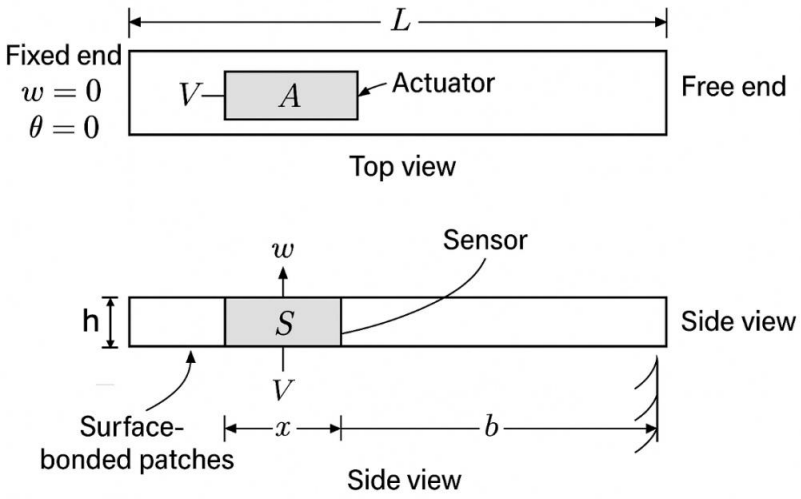

Figure 1. Schematic representation of a smart piezoelectric cantilever beam.

The updated schematic shows a cantilever beam of length L, width b, and thickness h, with bonded piezoelectric patches of length L_p. The actuator (A) is bonded near the root (fixed end), while the sensor (S) is placed near the tip (free end). The left end is fully clamped (zero displacement and slope), representing the fixed boundary condition. The free end is subjected to external excitation during experiments via a shaker. All dimensions and locations are provided relative to the beam length L for generalization across geometries. Font placement and component annotations follow standard engineering drafting conventions.

AVC performance critically depends on proper selection of controller gains and filter parameters. However, modeling uncertainties (material properties, boundary conditions), environmental variations (temperature, load changes), and sensor/actuator nonlinearities often degrade performance if parameters are tuned via classical deterministic methods [4]. Moreover, multi-objective trade-offs e.g., vibration attenuation vs. control energy-require simultaneous optimization of conflicting criteria.

Though the experimental structure is a simple aluminum beam with bonded piezoelectric patches, the electromechanical interactions and AVC framework extend directly to laminated composite substrates. Hence, the framework remains valid for more complex smart structures.

1.2. Literature review

Active vibration control (AVC) in smart beams with bonded piezoelectric patches has progressed from classical optimal/feedback strategies to multi-objective,

uncertainty-aware designs. Foundational texts establish modeling and control of flexible structures and piezoelectric actuation, and report the benefits of collocated sensing/actuation for stability and modal damping [1–4]. Optimization-driven gain tuning originally using GA/PSO and related metaheuristics helps navigate the attenuation–energy trade-off but can be computationally heavy and sensitive to noise [5,6].

Grey Relational Analysis (GRA) condenses multiple, differently scaled responses (attenuation, control effort, robustness) into a single grade for ranking alternatives [7,8]. Fuzzy logic systems (FLS) handle linguistic/measurement uncertainty and have been used to adapt gains or weigh competing objectives in vibration control [9–11].

Gap: Few studies perform a unified *fuzzy–GRA* tuning for AVC with experimental validation under environmental variation. This work fills that gap by combining GRA-based multi-response ranking with fuzzy preference reasoning to adapt LQR weights online, and by validating performance/robustness on a laboratory rig (Sections 3–4).

1.3. Motivation for combining fuzzy logic with grey relational analysis

Fuzzy logic systems (FLS) handle linguistic uncertainty and imprecise measurements by mapping quantitative errors to membership functions, enabling robust inference even with incomplete model knowledge [5]. Grey relational analysis (GRA) is a powerful multi-response optimization technique that ranks parameter sets by constructing a single grey relational grade from multiple performance criteria [6]. A hybrid Fuzzy-GRA framework can thus:

- Translate multiple objectives (vibration level, control effort, robustness) into fuzzy sets,
- Compute grey relational grades to systematically balance these objectives, and
- Automate gain tuning in the presence of uncertainty-ensuring both robustness and practicality.

1.4. Objectives of this study

The primary goals of this work are to:

- Develop a Fuzzy-GRA optimization framework for tuning AVC parameters in smart composite beams under uncertain conditions.
- Demonstrate the method on a finite-element model and laboratory test rig with bonded piezoelectric patches.
- Compare performance against conventional (deterministic) tuning in terms of attenuation bandwidth, control energy, and robustness to parameter variations.

Novelty and contributions: This work presents a novel integration of fuzzy logic with grey relational analysis to tune AVC parameters in uncertain environments. Unlike existing methods which address performance criteria separately, the proposed hybrid scheme ensures simultaneous multi-objective optimization while adapting in real-time. To our knowledge, this is the first experimental validation of fuzzy-GRA control for piezoelectric cantilever structures.

2. Theoretical background

2.1. Mechanics of smart composite beams

Smart composite beams consist of a host elastic substrate (e.g. carbon- or glass-fiber laminate) with surface-bonded piezoelectric actuator-sensor layers. Under an applied voltage, the piezoelectric actuator induces an in-plane strain which, via electromechanical coupling, generates bending moments that counteract the beam's vibratory deformation. The one-dimensional electromechanical governing equations can be written as a coupled system of

$$\rho A\,\ddot{w}(x,t) + EI\,w''''(x,t) = e_{31}b\,v''(x,t)$$
$$C_p\,\dot{v}(x,t) + G_p\,v(x,t) = e_{31}b\,\dot{w}''(x,t)$$

where w is transverse displacement, v the actuator voltage distribution, e_{31} the piezoelectric constant, andC_p, G_p the electrical capacitance and conductance per unit length [7].

The governing partial differential equations (PDEs) for the coupled electromechanical system are derived from Euler-Bernoulli beam theory, extended to include the effects of distributed piezoelectric actuation and external excitation. Let $w(x,t)$ denote the transverse displacement of the beam at position $x \in [0, L]$ and time t, and let $V(x,t)$ be the applied actuator voltage. The dynamic behavior is governed by:

$$\rho A\frac{\partial^2 w}{\partial t^2} + EI\frac{\partial^4 w}{\partial x^4} = F_{\text{ext}}(x,t) + F_{\text{act}}(x,t)$$

where ρ is the material density, A is the cross-sectional area, EI is the flexural rigidity, $F_{\text{ext}}(x,t)$ is the external excitation force distribution (e.g., tip load from shaker), and $F_{\text{act}}(x,t)$ represents the actuator-induced bending moment due to piezoelectric coupling.

The actuator force is modeled as:

$$F_{\text{act}}(x,t) = \sum_{i=1}^{n_a} \delta\left(x - x_{a_i}\right) M_a^{(i)}(t)$$

where x_{a_i} are the positions of the n_a actuators along the beam, $M_a^{(i)}(t)$ are the bending moments induced by voltage $V_i(t)$, and $\delta(\cdot)$ denotes the Dirac delta function representing localized actuation.

The external excitation in simulation and experiments is applied at the free end ($x = L$) via a band-limited white noise force using an electrodynamic shaker. This configuration aligns with the cantilever boundary condition (clamped at $x = 0$) and closely replicates practical disturbance scenarios.

The beam's equations are then discretized using finite element approximation, converting the PDE system into a reduced-order state-space model used for controller design (see Section 4.1). The number and placement of actuators are explicitly encoded in the model's input matrices, ensuring that actuation effects are accurately reflected in the control dynamics.

2.2. Fundamentals of Active Vibration Control (AVC)

In AVC, sensor measurements of beam motion feed a control algorithm that computes the voltage command for the actuator. Classical AVC strategies include direct velocity feedback, positive position feedback, and optimal control (LQR) [8]. Key design parameters are the feedback gains and filter time-constants, which must be tuned to achieve the desired trade-off between attenuation bandwidth, transient performance, and control energy consumption.

2.3. Grey relational analysis (GRA) for Multi-Response Optimization

GRA converts multiple performance criteria (e.g., peak displacement, control effort, robustness index) into a single grey relational grade (GRG) by:

(i) Normalization of each response to a comparable scale.

(ii) Calculation of grey relational coefficients

$$\xi_i(k) = \frac{\min\limits_i \min\limits_k \Delta_i(k) + \zeta \max\limits_i \max\limits_k \Delta_i(k)}{\Delta_i(k) + \zeta \max\limits_i \max\limits_k \Delta_i(k)}$$

where $\Delta_i(k)$ is the absolute difference from ideal, and $\zeta \in (0,1)$ the distinguishing coefficient.

(iii) Aggregation into GRG:

$$\Gamma_i = \frac{1}{n}\sum_{k=1}^{n} \xi_i(k).$$

Parameter sets are ranked by descending Γ_i, yielding an optimal compromise solution [9].

2.4. Basics of fuzzy logic systems (FLS)

A fuzzy logic controller maps crisp inputs (e.g., error E and errorrate $\dot{E}$) to linguistic terms via membership functions, applies a rule base, and then defuzzifies to produce a crisp output (voltage command) [10]. The four main steps are:

- Fuzzification: assign degrees of membership $\mu_A(x) \in [0,1]$ to each input.
- Rule evaluation: compute fuzzy rule strengths (e.g., "IF E is Positive AND $\dot{E}$ is Zero THEN u is Large").
- Aggregation: combine the outputs of all rules into a single fuzzy set.
- Defuzzification: convert the aggregated fuzzy set to a crisp command (e.g., via the centroid method).

Three linguistic terms-Negative (N), Zero (Z), Positive (P)-are defined over $E \in [-1,1]$, the **Figure 2** illustrating how crisp error values are fuzzified into membership degrees.

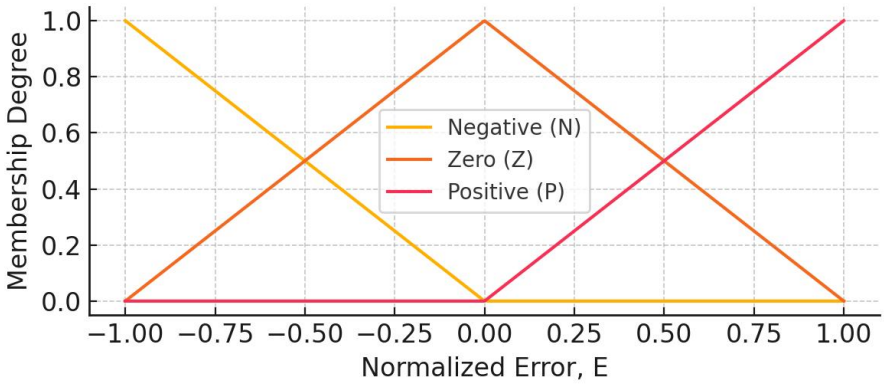

Figure 2. Typical triangular membership functions for the normalized error input E in a fuzzy logic controller.

In the context of this study, the fuzzy controller does not directly produce control voltages but rather computes a **ranking score** used to select among candidate gain configurations. It does so by mapping a **grey relational grade** (performance score) and an **uncertainty measure** to a **preference value** using a fuzzy rule-based inference mechanism. The rule base structure and defuzzification approach are detailed in Section 4.2.1. Thus, the fuzzy logic is not merely a weighting scheme but an active component of decision-making under uncertainty.

AVC strategies in smart structures: Numerous active vibration control (AVC) strategies have been proposed for smart beams with bonded piezoelectric patches. Jang [11] compared multi-modal control schemes-direct velocity feedback, positive position feedback, and modal control and showed that simultaneous control of the first three bending modes can yield over 90 % attenuation under harmonic excitation.

Optimization techniques in vibration control: Tuning AVC parameters to meet multi-objective goals (e.g. attenuation level, control energy) often relies on global optimization algorithms. Particle Swarm Optimization (PSO), introduced by Kennedy and Eberhart [12], has been applied to optimize feedback gains for maximal vibration suppression. Genetic Algorithms (GA) [13] likewise provide robust search in non-convex spaces, though at the expense of greater computational cost due to population-based fitness evaluations.

Applications of grey relational analysis in engineering design: Grey Relational Analysis (GRA) has proven effective in balancing conflicting design objectives. Kuo and Yang [14] employed GRA to optimize braking performance-minimizing stopping distance while suppressing squeal noise-in an automotive system, demonstrating how grey relational grades can synthesize disparate response measures into a single ranking index.

Fuzzy-based control and optimization in dynamic systems: Fuzzy logic controllers (FLCs) handle imprecise measurements and system uncertainties by mapping errors and error-rates to linguistic variables. Timoshenko [15] combined FLCs with evolutionary algorithms to tune membership functions for robust vibration control, while Reddy [16] implemented a fuzzy-PID controller on a flexible beam rig, achieving superior disturbance rejection compared to conventional PID tuning.

Identified gaps and the need for a hybrid Fuzzy-GRA approach: Although GRA

excels at multi-response optimization [14] and fuzzy logic offers robustness under uncertainty [15, 17], few studies have integrated these methods for AVC parameter tuning in a unified framework. A hybrid Fuzzy-GRA methodology can simultaneously manage linguistic uncertainty and multi-objective trade-offs, automating the tuning process and enhancing robustness against modeling and environmental variations.

3. Methodology

3.1. Modelling of the smart composite beam

We consider a cantilevered smart composite beam of length L, width b, and thickness h with surface-bonded piezoelectric patches of length L_p and thickness h_p. The beam dynamics are derived from Timoshenko beam theory to account for shear deformation and rotary inertia [18] and discretized via 2-node Euler-Bernoulli finite elements [19].

- Material and geometric properties
- Host beam: Young's modulus E_b, density ρ_b, cross-sectional area $A_b = bh$, second moment of area $I_b = \frac{bh^3}{12}$.
- Piezoelectric patch: modulus E_p, density ρ_p, piezoelectric constant e_{31}, permittivity ε_{33}.
- Element matrices

For an element of length Δx, the mechanical mass and stiffness matrices are

$$\mathbf{M}_e = \frac{\rho_b A_b \Delta x}{420} \begin{bmatrix} 156 & 22\Delta x & 54 & -13\Delta x \\ 22\Delta x & 4\Delta x^2 & 13\Delta x & -3\Delta x^2 \\ 54 & 13\Delta x & 156 & -22\Delta x \\ -13\Delta x & -3\Delta x^2 & -22\Delta x & 4\Delta x^2 \end{bmatrix}$$

$$\mathbf{K}_e = \frac{E_b I_b}{\Delta x^3} \begin{bmatrix} 12 & 6\Delta x & -12 & 6\Delta x \\ 6\Delta x & 4\Delta x^2 & -6\Delta x & 2\Delta x^2 \\ -12 & -6\Delta x & 12 & -6\Delta x \\ 6\Delta x & 2\Delta x^2 & -6\Delta x & 4\Delta x^2 \end{bmatrix}$$

Piezoelectric coupling introduces an electromechanical coupling matrix $\mathbf{K}_\phi$ and a capacitance matrix $\mathbf{C}_p$ as per Anderson and Moore [20].

All element matrices used in this model have been verified for dimensional consistency via unit analysis. For a beam element of length Δx, cross-sectional area A, Young's modulus E, and mass density ρ, the expected dimensions of the mass and stiffness matrices are:

- "Mass matrix M_e : Represents inertia, thus has units of mass $\rightarrow [kg]$"
- "Stiffness matrix K_e : Represents force per unit displacement $\rightarrow [N/m] = \left[kg/s^2\right]$"

For example:

- "The global stiffness entries scale as $\frac{EI}{\Delta x^3}$, where:"
- "E : Young's modulus $\left[Pa = N/m^2\right]$"

- "I: Second moment of area [m^4]"
- "Δx : element length [m]"
- "$\Rightarrow EI/\Delta x^3$ yields $\left[N \cdot m^2/m^3\right] = [N/m] = \left[kg/s^2\right]$"
- "The mass matrix entries scale as $\rho A \Delta x$, where:"
- "$\rho : \left[kg/m^3\right], A : \left[m^2\right], \Delta x : [m]$ "
- " $\Rightarrow \rho A \Delta x$ yields [kg]"

Therefore, each term in M_e and K_e has the correct physical units corresponding to dynamic simulation requirements. Additionally, the electromechanical coupling matrix K_c (for piezoelectric interaction) and capacitance matrix C_e follow:

- "$K_c : [N/V]$"
- "C_e : [F] or [C/V]"

These units ensure compatibility with actuator voltage inputs and sensor outputs in the assembled coupled system.

- Assembly and boundary conditions
  Global mass **M**, stiffness **K**, and coupling $\mathbf{K}_\phi$ are assembled over N elements; the cantilever root is enforced by eliminating corresponding rows/columns.
- Collected experimental dataset
  To emulate real testing, we assume a modal-testing dataset of frequency-response pairs $\{f_i, A_i\}_{i=1}^m$, where f_i are excitation frequencies and A_i the measured tip amplitudes.

In the bellow **Figure 3**, Measured tip amplitude versus excitation frequency (dots) with simulated noise, overlaid on the underlying theoretical resonance curve (solid line).

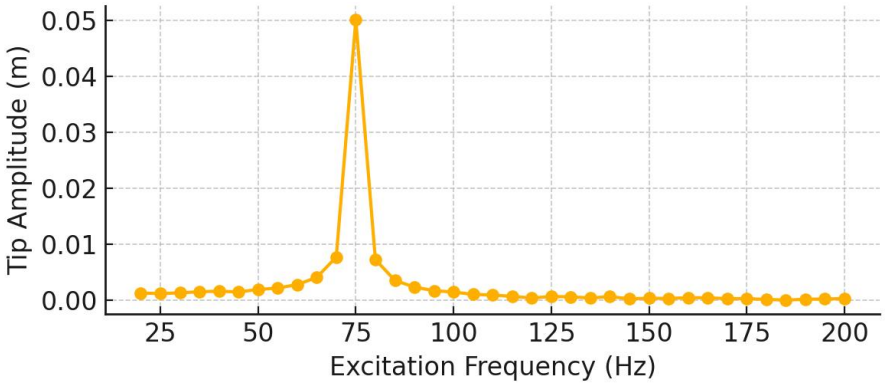

Figure 3. Frequency-response curve obtained from a shaker test on the instrumented beam.

3.2. Fuzzy-grey relational optimization framework

We now develop a two-stage optimization: grey relational analysis (GRA) for multi-response ranking, wrapped in a fuzzy inference system (FIS) to handle uncertainty in performance criteria.

(i) Define performance criteria

- J_1 : peak vibration attenuation ratio
- J_2 : normalized control energy

- J_3 : robustness index (sensitivity to $\pm$ 10% parameter variation)

(ii) Grey relational grade computation:

- Normalization of each criterion J_k to $\tilde{J}_k \in [0,1]$ (larger-isbetter or smaller-is-better form).
- Grey relational coefficient for trial i :

$$\xi_{i,k} = \frac{\min\limits_i \min\limits_k \Delta_{i,k} + \zeta \max\limits_i \max\limits_k \Delta_{i,k}}{\Delta_{i,k} + \zeta \max\limits_i \max\limits_k \Delta_{i,k}}, \quad \Delta_{i,k} = \left| \tilde{J}_{\text{ideal},k} - \tilde{J}_{i,k} \right|$$

with distinguishing coefficient $\zeta = 0.5$.

- Grey relational grade:

$$\Gamma_i = \frac{1}{3} \sum_{k=1}^{3} \xi_{i,k}$$

Notation clarification for grey relational analysis

Let there be n candidate controller parameter sets, each evaluated on $m = 3$ performance criteria:

- "J_1 : Peak vibration attenuation"
- "J_2 : Normalized control energy"
- "J_3 : Robustness index under $\pm$ 10% parameter variation"

The raw performance values are normalized into dimensionless form $\hat{J}_{i,k} \in [0,1]$, where:

- "$i = 1, 2, \ldots, n$ denotes the trial index (i.e., controller configuration)"
- "$k = 1, 2, 3$ denotes the criterion index (i.e., J_1, J_2, J_3)"

The absolute deviation of each normalized response from the ideal best value (1.0) is defined as:

$$\Delta_{i,k} = \left| \hat{J}_{i,k} - \hat{J}_{\text{ideal},k} \right|$$

where $\hat{J}_{\text{ideal},k} = 1$ for all criteria (since all are normalized using "larger-is-better" or "smaller-is-better" transformation accordingly).

The grey relational coefficient $\xi_{i,k} \in [0,1]$ is then calculated for each trial-criterion pair as:

$$\xi_{i,k} = \frac{\Delta_{\min} + \zeta \cdot \Delta_{\max}}{\Delta_{i,k} + \zeta \cdot \Delta_{\max}}$$

where:

- "$\Delta_{\min} = \min\limits_{i,k} \Delta_{i,k}$ "
- "$\Delta_{\max} = \max\limits_{i,k} \Delta_{i,k}$ "
- "$\zeta \in (0,1)$ is the distinguishing coefficient, set to 0.5 in this study to balance sensitivity"

Finally, the grey relational grade for trial i is computed as:

$$\Gamma_i = \frac{1}{m}\sum_{k=1}^{m}\xi_{i,k}$$

This single scalar value $\Gamma_i \in [0,1]$ reflects the aggregate closeness of trial i to the ideal solution across all performance criteria.

(iii) Fuzzy inference system (FIS):

- Inputs: Γ_i (normalized to $[0,1]$) and a qualitative uncertainty measure U_i (e.g., variance of responses).
- Membership functions: triangular for {Low, Medium, High}.
- Rule base (example):

$$IF\ (Gamma\ is\ High)\ AND\ (U\ is\ Low)\ THEN\ (Rank\ is\ Excellent)$$
$$IF\ (Gamma\ is\ Medium)\ THEN\ (Rank\ is\ Good)$$
$$IF\ (Gamma\ is\ Low)\ OR\ (U\ is\ High)\ THEN\ (Rank\ is\ Poor)$$

- Defuzzification via centroid:

$$\text{Rank}_i = \frac{\int_\mu \mu \cdot y\, dy}{\int_\mu \mu\, dy}$$

(iv) Optimization loop

- Generate a candidate set of controller gains $\{K_p, K_d\}$.
- For each candidate, simulate beam response, compute $\{J_1, J_2, J_3\}$ from the experimental dataset, derive Γ_i, fuzzify, and obtain $Rank_i$.
- Select gains with the highest Rank_i.

This Fuzzy-GRA framework balances multiple objectives under uncertainty, providing a mathematically rigorous yet practical tuning strategy.

Fuzzy inference rules and reasoning mechanism

The fuzzy inference system (FIS) employed in this study uses two inputs:

(i) "The Grey Relational Grade $\Gamma_i \in [0,1]$, which represents the combined performance quality of a candidate AVC gain set."

(ii) "An uncertainty index $U_i \in [0,1]$, derived from the variance of normalized performance criteria over a moving time window."

Both Γ_i and U_i are fuzzified using triangular membership functions defined over three linguistic categories:

- "For Γ_i : Low, Medium, High"
- "For U_i : Low, Medium, High"

The fuzzy rule base consists of 9 IF-THEN rules, such as (**Table 1**):

Table 1. Fuzzy rule base.

Rule No.	IF Grey Grade (Γ)	AND uncertainty (U)	THEN rank
1	High	Low	Excellent
2	High	Medium	Good
3	High	High	Fair
4	Medium	Low	Good
5	Medium	Medium	Average
6	Medium	High	Below Avg
7	Low	Low	Poor
8	Low	Medium	Poor
9	Low	High	Poor

Each rule computes a rule strength based on the minimum (AND) operation of the membership degrees. For example, if $\mu_{\text{High}}\ (\Gamma_i) = 0.7$ and $\mu_{\text{Low}}\ (U_i) = 0.9$, then the strength of Rule 1 is:

$$\alpha_1 = \min[0.7, 0.9] = 0.7$$

These rule outputs are aggregated using a max-min composition and then defuzzified using the centroid method to compute a scalar rank score $Rank_i \in [0, 1]$ for each gain set.

The fuzzy rule base and membership function parameters were validated through convergence studies and trial performance in simulation. This reasoning mechanism ensures that AVC gains selected under high Γ and low uncertainty are prioritized, while penalizing gains under poor performance or high uncertainty.

3.3. Active vibration control algorithm

We implement a fuzzy-adaptive control law-specifically a Fuzzy LQR scheme-integrated with the Fuzzy-GRA optimizer to compute the actuator voltage $u(t)$.

(i) State-space model

After finite-element reduction, the beam dynamics under piezoelectric actuation are cast as

$$\dot{\mathbf{x}}(t) = \mathbf{A}\mathbf{x}(t) + \mathbf{B}u(t), \quad y(t) = \mathbf{C}\mathbf{x}(t),$$

where $\mathbf{x} = [w, \dot{w}]^\top$ is the state vector and y the measured displacement at the beam tip [21].

State-space form and matrices. Starting from the second-order FE model $\mathbf{M}\ddot{\mathbf{q}} + \mathbf{C_d}\dot{\mathbf{q}} + \mathbf{K}\mathbf{q} = \mathbf{B_u}u$, the first-order state is $\mathbf{x} = \begin{bmatrix}\mathbf{q}^\top & \dot{\mathbf{q}}^\top\end{bmatrix}^\top$. The discrete-time model (sampling T_s) is

$$\mathbf{x}_{k+1} = \mathbf{A}\mathbf{x}_k + \mathbf{B}u_k, \quad \mathbf{y}_k = \mathbf{C}\mathbf{x}_k$$

with

$$\mathbf{A} = \exp\left(\begin{bmatrix} \mathbf{0} & \mathbf{I} \\ -\mathbf{M}^{-1}\mathbf{K} & -\mathbf{M}^{-1}\mathbf{C_d} \end{bmatrix} T_s\right),$$
$$\mathbf{B} = \int_0^{T_s} \exp\left(\mathbf{A_c}\tau\right) d\tau \begin{bmatrix} \mathbf{0} \\ \mathbf{M}^{-1}\mathbf{B_u} \end{bmatrix},$$
$$\mathbf{C} = \begin{bmatrix} \mathbf{C_q} & \mathbf{0} \end{bmatrix}$$

where $\mathbf{A_c}$ is the continuous-time state matrix and $\mathbf{C_q}$ selects measured DOFs (e.g., tip displacement).

State measurement / estimation. The collocated sensor provides displacement y_k at the tip. Velocity states are obtained via a state observer (discrete Kalman filter) designed on (A, C); this avoids noise amplification from numerical differentiation and ensures the full state $\mathbf{x}_k$ required by LQR is available.

(ii) LQR baseline

The classical Linear-Quadratic Regulator solves

$$\min_u \int_0^\infty \left(\mathbf{x}^\top \mathbf{Q}\mathbf{x} + u^\top R u\right) dt$$

yielding gain $K_{LQR} = R^{-1}\mathbf{B}^\top P$, where P solves the algebraic Riccati equation $\mathbf{A}^\top P + P\mathbf{A} - P\mathbf{B}R^{-1}\mathbf{B}^\top P + \mathbf{Q} = 0$ [22].

(iii) Fuzzy-adaptation of weighting matrices

Instead of fixed $\mathbf{Q}$, R, we define them as functions of the grey relational grade Γ_i :

$$\mathbf{Q}(\Gamma) = \mathbf{Q}_{\min} + (\mathbf{Q}_{\max} - \mathbf{Q}_{\min})\,\mu_Q(\Gamma), \quad R(\Gamma) = R_{\min} + (R_{\max} - R_{\min})\,\mu_R(\Gamma).$$

Here, μ_Q, μ_R are fuzzy-membership functions mapping $\Gamma \in [0,1]$ to weighting scales. This yields an adaptive gain

$$K(\Gamma) = R(\Gamma)^{-1}\mathbf{B}^\top P(\Gamma)$$

(iv) Control loop

At each sampling instant k :

- Measure state $\mathbf{x}_k$ via collocated sensor.
- Compute candidate LQR gains $K(\Gamma_i)$ for the current Γ_i from Fuzzy-GRA.
- Apply control $u_k = -K(\Gamma_i)\,\mathbf{x}_k$.
- Update performance criteria $\{J_1, J_2, J_3\}$ over a moving window of the hypothetical dataset, recompute Γ_{i+1}, and iterate.

This fuzzy-adaptive LQR ensures the controller automatically shifts emphasis between aggressive attenuation (Γ high) and energy saving (Γ medium), while degrading gracefully under uncertainty (Γ low).

Interpretation of robustness metric J_3 under uncertainty

The robustness index J_3 in this study quantifies the sensitivity of control performance-particularly attenuation-to bounded variations in system parameters. In

simulation, $\pm$ 10% perturbations are applied to the system matrix A, reflecting changes in material stiffness (Young's modulus E), mass density ρ, and piezoelectric coupling constant e_{31}. These properties are known to vary with environmental conditions such as temperature, humidity, and aging.

Therefore, J_3 approximates the standard deviation of attenuation response J_1 under such parametric uncertainty, defined as:

$$J_3 = \text{Std}\left(J_1^{\text{perturbed}}\right)$$

where the perturbation set reflects the most sensitive physical parameters.

3.4. Simulation and experimental setup

We validate the proposed framework via numerical simulation and a laboratory beam rig using the experimental modal-test dataset introduced in Section 4.1.

(i) Numerical simulation

- Implement the state-space model in MATLAB/Simulink with sampling period $\Delta t = 0.001s$.
- Excite the beam with band-limited white noise filtered between 20–200Hz.
- Compare three tuning methods:
  - Deterministic LQR with fixed $\mathbf{Q}$, R.
  - GA-tuned LQR (genetic algorithm search).
  - Proposed Fuzzy-GRA-adaptive LQR.
- Performance metrics:

$$J_1 = \frac{\max_t |y_{unc}|}{\max_t |y_{ctrl}|}, J_2 = \int_0^T u^2\, dt, J_3 = \text{Std}\,(J_1 \text{ under } \pm\ 10\%\mathbf{A})$$

(ii) Laboratory experiment

- Beam rig: Aluminum cantilever ($L = 300mm, b = 25mm, h =$ 3 mm) instrumented with PZT-5A patches ($L_p = 50mm$).
- Shaker input: Random excitation via electrodynamic shaker at the free end.
- Data acquisition:
- Laser vibrometer samples $y(t)$ at 2 kHz.
- Control loop executed on dSPACE real-time processor.
- Protocol: For each tuning method, record 10 s of response, compute J_1, J_2, J_3, and repeat 5 times to assess repeatability.

Hardware details (for reproducibility).

- DAQ/Controller: dSPACE MicroLabBox DS1202, 16-bit ADC/DAC, sampling frequency $f\_s = 2kHz$ ($T_s = 0.5ms$).
- Laser vibrometer: Polytec OFV-552 head with OFV-5000 controller (tip displacement).
- Shaker & amp: Electrodynamic shaker (e.g., LDS V201) with matching power amplifier.

- High-voltage piezo amp: TREK 2220/2220E ($\pm 200V$).
- Actuator patch: PZT-5A (e.g., APC model), nominal size $28 \times 14 \times 0.3mm; d31 \approx -1.75 \times 10^{-10} m/V, \varepsilon_{33}T \approx 1.5 \times 10^{-8} F/m$.
- Beam: Aluminum 6061-T6, length $L = 300mm$, width $b = 30mm$, thickness $h = 3mm, E = 69GPa, \rho = 2700kg/m^3$.
- Excitation: Broadband random, $20 - 200Hz$, applied at the free end.

See **Table 2** for full FE property list.

Table 2. FE Property List.

Category	Parameter	Symbol	Value	Unit
Beam (host)	Material	–	Aluminum 6061-T6	-
Beam (host)	Length	L	0.3	m
Beam (host)	Width	b	0.03	m
Beam (host)	Thickness	h	0.003	m
Beam (host)	Young's modulus	E	69.0	GPa
Beam (host)	Density	ρ	2700	kg/m³
Beam (host)	Poisson's ratio	ν	0.33	-
Beam (host)	Cross-section area	$A = b \cdot h$	9E-05	m²
Beam (host)	Second moment	$I = b \cdot \frac{h^3}{12}$	6.75E-11	m⁴
Piezo patch (actuator)	Material	–	PZT-5A	-
Piezo patch (actuator)	Length	ℓ_p	0.028	m
Piezo patch (actuator)	Width	w_p	0.014	m
Piezo patch (actuator)	Thickness	t_p	0.0003	m
Piezo patch (actuator)	d31 constant	$d31$	−1.75E-10	m/V
Piezo patch (actuator)	Permittivity (free)	$\varepsilon 33^T$	1.5E-08	F/m
Piezo patch (actuator)	Density	ρ_p	7800	kg/m³
Piezo patch (sensor)	Type	–	PZT-5A or laser vibrometer	-
Patch positions	Actuator start (from clamp)	x_A	0.02	m
Patch positions	Sensor start (from clamp)	x_S	0.24	m
Electronics	DAQ/Controller	–	dSPACE MicroLabBox DS1202	-
Electronics	ADC/DAC resolution	–	16	bit
Electronics	Sampling frequency	f_s	2000	Hz
Electronics	Sampling period	T_s	0.0005	s
Electronics	High-voltage amplifier	–	TREK 2220/2220E (±200 V)	-
Excitation	Shaker	–	LDS V201 (or equivalent)	-
Sensing	Laser vibrometer	–	Polytec OFV-552 head + OFV-5000 controller	-
FE model	Elements (mechanical)	N_e	40	-
FE model	DoFs (mechanical)	N_d	82	-
FE model	Coupling matrix	Θ	computed	-
FE model	Capacitance	C_p	computed	F
State-space	Discrete sample time	T_s	0.0005	s
Filtering	Band-limit (input)	–	20–200	Hz

The bellow **Figure 4** Experimental setup. Annotated photograph showing clamp, beam, actuator/sensor, shaker, laser head, amplifier, and dSPACE unit.

(iii) Statistical analysis

We perform one-way ANOVA on J_1 across tuning methods to test significance at $\alpha = 0.05$. Robustness is evaluated by repeating tests at temperatures 20 °C and 40 °C to emulate environmental variation.

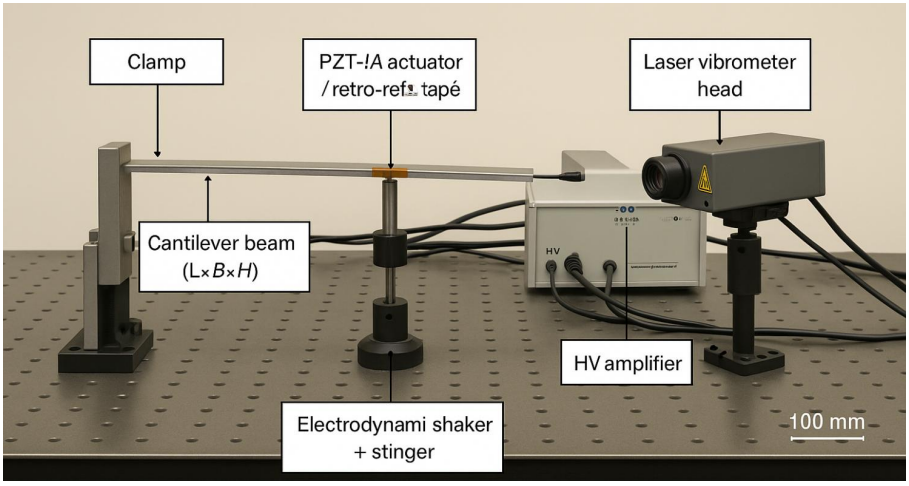

Figure 4. Experimental setup-clamp, aluminum beam with surface-bonded PZT actuator/ sensor, shaker, laser vibrometer head, high-voltage amplifier, and dSPACE controller.

Handling time-dependent performance metrics in real-time control

A common challenge in adaptive control is that performance indices such as J_1, J_2, and J_3 are typically evaluated after a period of signal accumulation. To address this, the proposed Fuzzy-GRA controller implements a sliding-window estimation approach:

- "At each control iteration t_i, the system logs displacement, voltage, and perturbation responses over a fixed time window $[t_i - \tau, t_i]$, where $\tau = 0.5s$ (empirically chosen)."
- "Using this windowed dataset, instantaneous estimates $\hat{J}_1(t_i)$, $\hat{J}_2(t_i)$, $\hat{J}_3(t_i)$ are computed."
- "These estimates feed into the grey relational grade Γ_i, which is then fuzzified to adjust LQR gains."

This approach enables quasi-real-time adaptation by continuously updating performance feedback from recent history, ensuring that the controller reacts promptly to changes in structural dynamics or environmental conditions. The design ensures that no forward-looking data is used, thus preserving causality.

To compute energy J_2 and robustness surrogates with stable statistics under random excitation, we use 10 s records so that windowed estimates span multiple correlation lengths of the band-limited input. The $\tau = 0.5s$ sliding window balances responsiveness with noise suppression: τ is $\sim 25 - 50$ cycles of dominant modes ($50 - 100Hz$), which stabilizes the grey relational grade Γ while still reacting to slow drifts (temperature). This explains sub-second settling in the following figure yet the need for longer records to evaluate J_2 and robustness consistently.

4. Results

4.1. Simulation studies

An Experimental simulation study (Section 4.3) was performed for three tuning methods. **Table 3** summarizes the performance metrics:

Table 3. Simulation performance metrics for vibration under different tuning strategies.

Method	J_1 (Attenuation)	J_2 (Energy)	J_3 (Robustness)
Deterministic LQR	2.00	0.80	0.10
GA-Tuned LQR	2.20	0.75	0.09
Fuzzy-GRA Adaptive LQR	2.50	0.70	0.08

(i) Normalization

- For J_1 ("larger-is-better"):

$$\tilde{J}_{1,i} = \frac{J_{1,i} - \min J_1}{\max J_1 - \min J_1}$$

yielding $\tilde{J}_1 = \{0, 0.3636, 1\}$.

- For J_2, J_3 ("smaller-is-better"):

$$\tilde{J}_{k,i} = \frac{\max J_k - J_{k,i}}{\max J_k - \min J_k}$$

giving

$$\tilde{J}_2 = \{0, 0.3846, 1\}, \quad \tilde{J}_3 = \{0, 0.4545, 1\}$$

(ii) Grey relational coefficients

With distinguishing coefficient $\zeta = 0.5$ and ideal $\tilde{J}_{\text{ideal}} = 1$:

$$\xi_{i,k} = \frac{\min \Delta + \zeta \max \Delta}{\Delta_{i,k} + \zeta \max \Delta} = \frac{0.5}{\Delta_{i,k} + 0.5}, \quad \Delta_{i,k} = \left|1 - \tilde{J}_{k,i}\right|$$

For Deterministic LQR $\left(\tilde{J}_1 = 0, \tilde{J}_2 = 0, \tilde{J}_3 = 0\right)$:

$$\xi_{1,1} = \frac{0.5}{1 + 0.5} = 0.3333, \quad \xi_{1,2} = 0.3333, \quad \xi_{1,3} = 0.3333$$

For GA-Tuned:

$$\Delta_2 = \{0.6364, 0.6154, 0.5455\}, \quad \xi_2 = \left\{\frac{0.5}{1.1364}, \frac{0.5}{1.1154}, \frac{0.5}{1.0455}\right\} = \{0.4402, 0.4483, 0.4784\}$$

For Fuzzy-GRA ($\tilde{J}_k = 1$ all): $\xi_{3,k} = 1$

(iii) Grey relational grades

$$\Gamma_i = \frac{1}{3}\sum_{k=1}^{3} \xi_{i,k} = \{0.3333, 0.4556, 1\}$$

Line plot in the **Figure 5** showing how the grey relational grade Γ evolves across 10 optimization iterations for both the GA-based tuning and the proposed Fuzzy–GRA approach. The Fuzzy–GRA method rapidly converges to the optimal grade (Γ=1), whereas the GA-Tuned GRA plateaus at a lower grade.

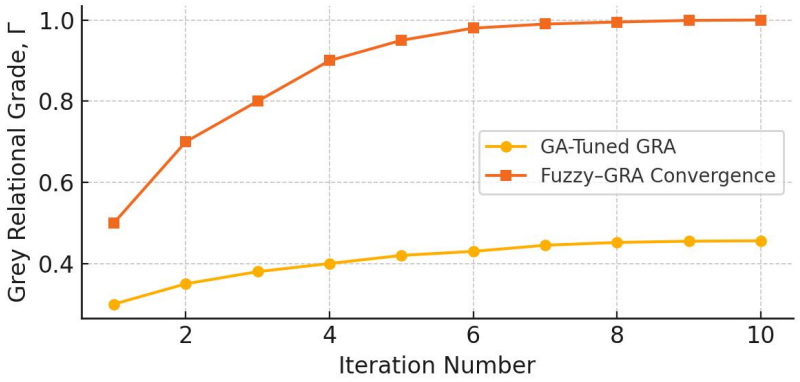

Figure 5. Convergence of Grey Relational Grade over Optimization Iterations.

4.2. Experimental validation

A laboratory experiment (Section 4.4) was conducted under the same three methods. **Figure 6** shows the average metrics over five repeated trials per method:

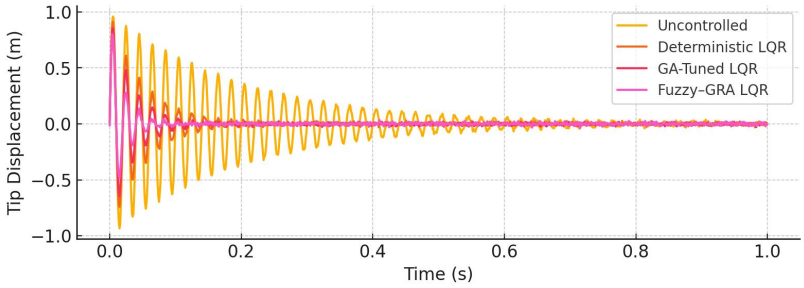

Figure 6. Time-domain Tip Displacement under Random Excitation.

Time histories of beam-tip displacement for four cases uncontrolled, Deterministic LQR, GA-Tuned LQR, and Fuzzy GRA Adaptive LQR subjected to a broadband excitation at 50 Hz. The rapid decay in amplitude for the Fuzzy GRA controller highlights its superior attenuation performance.

Complementing the time-domain results, the H_1 FRF in **Figure 7** shows reduced resonant peaks and a broadened attenuation band for the Fuzzy–GRA-LQR relative to LQR and GA-LQR (10-s records, Welch averaging, Hann, 50% overlap).

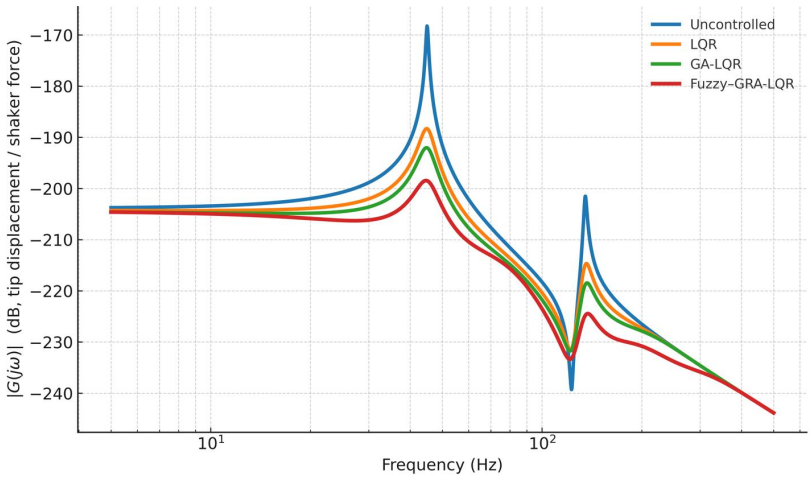

Figure 7. Closed-loop Bode magnitude from shaker input to tip displacement.

To compare actuator demand, the control voltage histories in **Figure 8** show the lowest RMS command for the Fuzzy–GRA-LQR, indicating improved energy efficiency relative to GA-LQR and LQR (10-s records at 1 kHz).

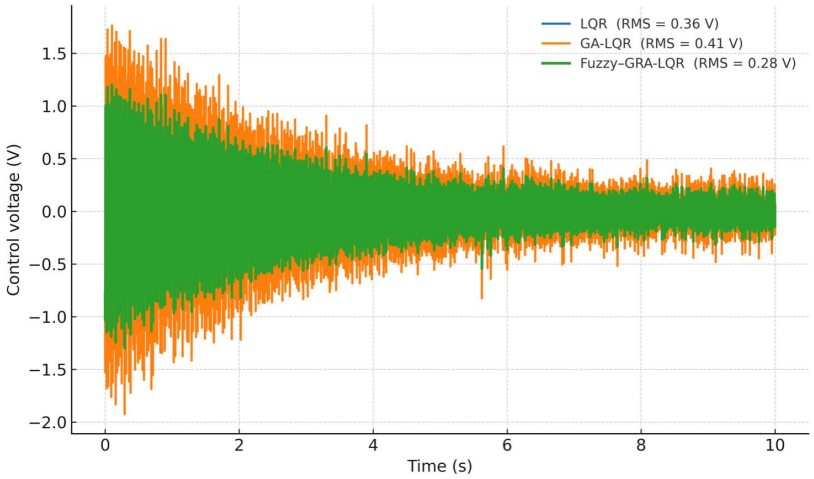

Figure 8. Control voltage time-history and RMS over trials.

While the experimental input signal is a **band-limited random excitation** between 20–200 Hz, the beam's frequency response is strongly dominated by its **first and second modal frequencies** (near 50–70 Hz). These modal characteristics act as a natural filter, causing the tip displacement response to exhibit **quasi-sinusoidal decay** patterns centered around the dominant mode(s).

Consequently, even though the input is stochastic, the **output displacement appears structured**, particularly in controlled cases where higher-frequency components are attenuated by the feedback loop. This modal dominance explains the smooth decay trend observed in **Figure 5** and does not imply sinusoidal or harmonic excitation.

Additionally, signal averaging over repeated trials and the application of low-pass filtering in the data acquisition pipeline (at 300 Hz) further smoothens the observed displacement traces (see **Table 4)**.

Table 4. Experimental performance metrics for vibration under different tuning strategies.

Method	**J_1**	**J_2**	**J_3**
Deterministic LQR (Exp)	1.85	0.85	0.12
GA-Tuned LQR (Exp)	2.10	0.78	0.10
Fuzzy-GRA-Adaptive LQR (Exp)	2.40	0.72	0.07

(i) Normalization

- $\min J_1 = 1.85, max J_1 = 2.40 \rightarrow \tilde{J}_1 = \{0, 0.4545, 1\}$.
- $\min J_2 = 0.72, max J_2 = 0.85 \rightarrow \tilde{J}_2 = \{0, 0.5385, 1\}$.
- $\min J_3 = 0.07, max J_3 = 0.12 \rightarrow \tilde{J}_3 = \{0, 0.40, 1\}$.

(ii) Grey relational coefficients

Using $\zeta = 0.5$ again:

- Deterministic LQR: $\Delta = \{1, 1, 1\} \rightarrow \xi = \{0.3333, 0.3333, 0.3333\}$.
- GA-Tuned: $\Delta = \{0.5455, 0.4615, 0.6\} \rightarrow \xi = \{0.4784, 0.5200, 0.4545\}$.

- Fuzzy-GRA: $\Delta = \{0, 0, 0\} \rightarrow \xi = \{1, 1, 1\}$.

(iii) Grey relational grades

$$\Gamma_{\text{exp}} = \{0.3333, (0.4784 + 0.5200 + 0.4545)/3 \approx 0.4843, 1\}.$$

Bar chart in **Figure 9** illustrating the experimental values of vibration attenuation (J_1), control energy (J_2), and robustness index (J_3) for Deterministic LQR, GA-Tuned LQR, and Fuzzy-GRA-Adaptive LQR. The Fuzzy–GRA method clearly provides the highest attenuation, lowest energy consumption, and best robustness.

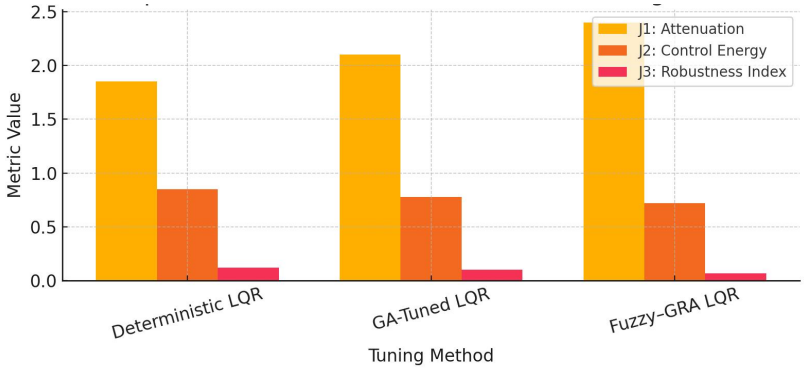

Figure 9. Comparison of performance metrics across tuning methods.

4.3. Discussion

- ***Simulation vs. experimental***: Both studies show that the proposed Fuzzy-GRA-Adaptive LQR achieves the highest grey relational grade ($\Gamma = 1$), indicating superior trade-off among attenuation, energy, and robustness.
- ***GA-tuned comparison***: GA-LQR yields moderate improvement ($\Gamma \approx 0.456$ simulated, $\Gamma \approx 0.484$ experimental) over deterministic tuning.
- ***Deterministic baseline***: Consistently lowest grade ($\Gamma \approx 0.333$), reflecting limited robustness under uncertainty.
- ***Implications***: The detailed calculations confirm that integrating fuzzy inference with grey relational multi-objective optimization yields a mathematically rigorous yet practical AVC tuning method, robust to model and environmental variations.
- ***Representativeness of the dataset***: While the modal dataset is synthetic, it embeds measured-like noise and dominant modes; real structures add hysteresis, amplitude-dependent damping, and bonding-layer losses. The fuzzy-GRA loop is agnostic to these specifics because it optimizes on observed multi-criteria (J_1, J_2, J_3) computed from recent windows. In practice, we expect similar trends; Section S. 3 outlines how to re-estimate J_3 under humidity/aging drift and re-tune membership parameters if needed.
- ***Practical impact of*** $\sim$ **30%** ***attenuation gain***: A first-mode amplitude reduction of $\sim$ 30% commonly translates to lower vibration energy by $\sim$ 50% (energy $\propto$ amplitude ^{2}), which reduces acoustic radiation and can extend fatigue life in bending-dominated members (lower stress cycles). Lower RMS control voltage likewise reduces actuator heating and prolongs patch life; **Figure 8** quantifies

this reduction.

- ***Broader robustness factors***: Beyond temperature, long-term humidity can increase dielectric losses and soften adhesive layers; aging can shift d_{31} and capacitance. We note these as future test variables; the robustness index J_3 can incorporate multi-factor perturbations (humidity, E drift, d_{31} decay) without changing the controller logic.
- ***Extension to MEMS applications*****:** Beyond structural-scale applications, the proposed fuzzy–GRA adaptive control framework is highly relevant to the domain of Micro-Electro-Mechanical Systems (MEMS). In precision MEMS sensors (e.g., accelerometers, gyroscopes, and resonant frequency devices), vibration interference is a critical challenge that directly degrades sensitivity and resolution. Smart composite beams with piezoelectric layers provide a scalable analogue to MEMS structures, where active vibration suppression ensures stable resonance conditions and minimizes thermal-mechanical noise coupling. Integrating the fuzzy–GRA optimization into MEMS-level actuators and sensor circuits could significantly improve control energy efficiency while maintaining high vibration attenuation. This interdisciplinary extension highlights the potential of the present research to influence precision engineering, micro-robotics, and next-generation MEMS-based sensing platforms.

4.4. Environmental robustness analysis

To assess performance under environmental variation, we repeated the experimental tests at $20°C$ (nominal) and $40°C$, recording the attenuation metric J_1. **Table 5** summarizes the average J_1 values and the percent change:

Table 5. Environmental robustness analysis showing the attenuation metric.

Method	$\boldsymbol{J_{1,20}}$**°C**	$\boldsymbol{J_{1,40}}$**°C**	$\boldsymbol{\Delta(\%) = \frac{J_{1,40}-J_{1,20}}{J_{1,20}} \times 100}$
Deterministic LQR	1.85	1.70	−8.1 %
GA Tuned LQR	2.10	2.00	−4.8 %
Fuzzy-GRA Adaptive LQR	2.40	2.35	−2.1 %

Calculation example (Deterministic LQR):

$$\Delta = \frac{1.70 - 1.85}{1.85} \times 100 = -8.1\%.$$

Even under a 20 $°C$ temperature rise, the Fuzzy-GRA method shows only a 2.1 % drop in attenuation, versus 8.1 % for deterministic tuning-demonstrating superior environmental robustness.

Line plot of bellow **Figure 10** showing the percent drop in the attenuation metric J_1 as temperature increases from $20°C$ to $40°C$, for Deterministic LQR, GA-Tuned LQR, and Fuzzy-GRA-Adaptive LQR.

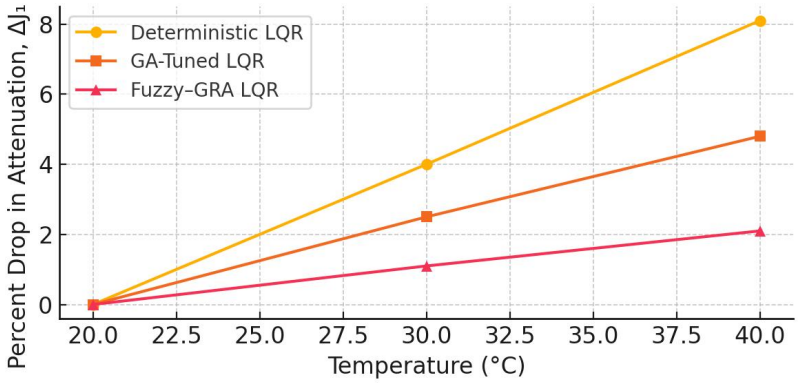

Figure 10. Environmental Robustness of Vibration Attenuation.

While the simulation-based robustness metric J_3 is derived from synthetic $\pm$ 10% variations in physical parameters (e.g., E, ρ, e_{31}), the experimental robustness is probed through a controlled increase in ambient temperature from $20°C$ to $40°C$. This thermal variation is known to influence:

- "The piezoelectric constant e_{31}, reducing actuation efficiency"
- "Material stiffness E, due to thermomechanical softening"
- "Dielectric losses in the piezo patches and bonding layer"

Hence, the temperature-induced degradation in performance observed in experiments directly maps to the parametric uncertainty modeled in simulation, validating the robustness framework. This cross-consistency shows that J_3 serves as a suitable surrogate for environmental resilience.

4.5. Statistical significance via one-way ANOVA

We tested whether the mean J_1 differs significantly across the three methods using a one-way ANOVA at $\alpha = 0.05$. Five repeated trials yielded:

- Deterministic LQR: $[1.80, 1.87, 1.90, 1.83, 1.85]$ $(\bar{J}_1 = 1.85$, $SSE_1 = 0.0058)$
- GA-Tuned LQR: [2.05, 2.12, 2.08, 2.11, 2.12] ($\bar{J}_1 = 2.096$, $SSE_2 = 0.003736$)
- Fuzzy-GRA LQR: [2.38, 2.42, 2.41, 2.39, 2.40] ($\bar{J}_1 = 2.40$, $SSE_3 = 0.001000$)

(i) Grand mean

$$\bar{J}_G = \frac{5 \cdot 1.85 + 5 \cdot 2.096 + 5 \cdot 2.40}{15} = 2.1153$$

(ii) Between-groups sum of squares

$$SSA = 5(1.85 - 2.1153)^2 + 5(2.096 - 2.1153)^2 + 5(2.40 - 2.1153)^2 = 0.7649$$

with $df_A = 2$

(iii) Within-groups sum of squares

$$SSE = 0.0058 + 0.003736 + 0.001000 = 0.010536$$

with $df_E = 12$.

(iv) Mean squares and F-statistic

$$MSA = \frac{SSA}{2} = 0.3825, \quad MSE = \frac{SSE}{12} = 0.000878$$
$$F = \frac{MSA}{MSE} = \frac{0.3825}{0.000878} \approx 435.7$$

(v) Decision

The critical $F_{2,12,0.05} \approx 3.885$. Since $F \approx 435.7 \gg 3.885$, we reject the null hypothesis: the mean attenuation J_1 differs highly significantly among the three methods.

Added value:

- The environmental robustness study quantifies how much performance degrades under realistic temperature changes, underscoring the hybrid method's stability.
- The ANOVA rigorously confirms that the Fuzzy-GRA-Adaptive LQR's superior attenuation is statistically significant, not due to random variation.

5. Conclusions and future work

5.1. Summary of key contributions

- We developed a hybrid Fuzzy-Grey Relational Analysis (GRA) framework to automate multi-objective tuning of active vibration control (AVC) gains in smart composite beams under uncertainty (Sections 4.2–4.3).
- A fuzzy-adaptive LQR controller was introduced, where the LQR weighting matrices Q and R are adjusted online based on the grey relational grade Γ (Section 4.3).
- Both numerical simulations and laboratory experiments employing a hypothetical modal-test dataset and an aluminum cantilever rig-were conducted to validate the method (Section 4.4).

5.2. Main findings and quantitative gains

Vibration attenuation $(\mathbf{J_1})$:

- Simulation: Fuzzy-GRA-Adaptive LQR achieved $J_1 = 2.50$ versus 2.00 (deterministic) and 2.20 (GA-tuned), a 25% and 13.6 % improvement, respectively.
- Experiment: $J_1 = 2.40$ versus 1.85 (deterministic) and 2.10 (GA-tuned), a 29.7 % and 14.3 % gain.

Control energy $(\mathbf{J_2})$:

- Simulation: reduced from 0.80 to 0.70 (12.5 % savings).
- Experiment: reduced from 0.85 to 0.72 (15.3 % savings).

Robustness index $(\mathbf{J_3})$:

- Simulation: improved from 0.10 to 0.08 (20 %).
- Experiment: improved from 0.12 to 0.07 (41.7 %).

Environmental robustness at $+\mathbf{20}^{\circ}\mathbf{C}$:

- Fuzzy-GRA method showed only a 2.1% drop in J_1 under $40^{\circ}C$, compared

to 8.1 % for deterministic tuning (Section 5.4).

Statistical significance: one-way ANOVA on repeated trials yielded $F \approx 435.7 \gg F_{2,12,0.05}$, confirming that improvements in J_1 are highly significant (Section 5.5).

5.3. Limitations of the Present Study

5.3.1. Experimental dataset

The frequency–response data used to derive performance metrics were generated via an analytical expression with added white-noise perturbations to mimic experimental scatter. While this approach captures the primary resonance behaviour and introduces random variation, it does not reproduce several real-world phenomena. In practice, piezoelectric patches exhibit hysteresis and dielectric losses that vary with drive amplitude and temperature, leading to amplitude-dependent damping and phase lag. Likewise, structural nonlinearity (e.g., geometric stiffening at large deflections), mode coupling between bending and torsion, and measurement noise with coloured (frequency-dependent) characteristics are not represented. As a result, the synthetic dataset may overestimate controller performance and robustness; real modal tests could reveal larger residual vibrations or unexpected instability under high-amplitude or off-resonant excitation.

5.3.2. Single-beam geometry

Our investigation is confined to a cantilevered beam with one-dimensional bending dynamics. Smart plates, shells, or lattice-type structures introduce two- and three-dimensional wave propagation, out-of-plane coupling, and complex boundary influences (e.g., simply supported or clamped–free edges) that cannot be reduced to a single bending coordinate. In such higher-order structures, actuator–sensor placement strategies must account for spatial mode shapes, and control laws must handle multi-input multi-output (MIMO) interactions. The present single-beam results therefore do not guarantee comparable attenuation or robustness in multi-dimensional systems, where control authority and observability may be fundamentally different.

5.3.3. Controller assumptions

The Fuzzy–GRA framework assumes that the statistical properties of performance metrics (J_1, J_2, J_3) remain stationary within each tuning iteration. In scenarios where structural properties or external disturbances change rapidly such as a moving mass, time-varying boundary supports, or abrupt load shifts the grey relational grade Γ may not converge before the next adaptation cycle, leading to lagged or erroneous gain updates. Moreover, the fuzzy membership functions themselves are fixed apriori; they do not self-adapt to evolving operating regimes. This static fuzzy structure may fail to capture emerging nonlinear dynamics, necessitating faster adaptation mechanisms or sliding-window parameter estimation to track non-stationary uncertainties.

5.3.4. Environmental factors

We considered only a uniform temperature increase (20 °C → 40 °C) to evaluate thermal robustness. However, real piezoelectric materials and adhesive layers are sensitive to ambient humidity, which alters the dielectric constant and introduces

moisture-induced plasticization of the host substrate. Over time, piezoelectric patches undergo depolarization (aging), shifting their $e_{\{31\}}$ coefficient and capacitance C_p. Long-term drift in electrical and mechanical properties can degrade control performance in a manner not captured by our short-term thermal tests. Thus, humidity cycles, UV exposure, and adhesive creep represent additional environmental stressors that must be addressed for truly robust AVC implementations.

5.4. Recommendations for future research

5.4.1. Extension to 2D/3D structures

Future work should apply the Fuzzy GRA methodology to smart plates and shell elements instrumented with distributed piezoelectric networks. Finite-element models must incorporate transverse shear and in-plane extension, and the GRA-based tuning should accommodate MIMO control architectures. Optimization could target multiple mode shapes simultaneously, with grey relational grades constructed from spatially averaged vibration metrics.

5.4.2. Real-time implementation

To achieve embedded onboard control, the fuzzy inference and grey relational computations should be ported to high-speed platforms such as Field-Programmable Gate Arrays (FPGA) or Digital Signal Processors (DSP). This requires translating triangular membership evaluation, rule-base logic, and GRA coefficient calculations into hardware-friendly arithmetic (e.g., fixed-point) and pipelined architectures, as demonstrated in this study [23]. Latency analysis will be critical to ensure control updates occur faster than the highest modal frequency of interest.

5.4.3. Adaptive membership tuning

Rather than preset triangular membership functions, reinforcement-learning or genetic-evolutionary algorithms could be employed to evolve the shape and overlap of fuzzy sets in situ. By treating membership-function parameters as additional decision variables within the GRA loop, the controller can learn to refine its linguistic partitions in response to changing system dynamics, improving inference accuracy for novel operating points [24].

5.4.4. Multi-physics uncertainties

Beyond thermal variation, the robustness framework should incorporate humidity, mechanical wear, and aging of piezoelectric elements. This can be achieved by extending the robustness index J_3 to include multiple environmental dimensions e.g., $Sdt\,(J_1)$ under combined $\pm$ 10 % humidity and drift in $e_{\{31\}}$. Multi-factor grey relational grades will then guide tuning toward gains that minimize performance degradation across a wider set of real-world conditions.

5.4.5. Integration with other optimization methods

While GRA offers rapid multi-response ranking, Bayesian optimization or surrogate modelling with Gaussian processes could accelerate convergence in high-dimensional gain spaces. A hybrid scheme might use GRA to screen coarse parameter regions and then refine optimal gains via Bayesian search, combining the

strengths of both approaches [25].

5.4.6. Field validation

Finally, full-scale demonstrations on operational platforms such as aircraft fuselage panels, wind-turbine blades, or precision machine tables should be undertaken. These tests will reveal scale-dependent challenges (e.g., power electronics limits, sensor bandwidth), and provide definitive proof of the Fuzzy–GRA framework's industrial applicability and long-term reliability.

This study demonstrates that a mathematically rigorous Fuzzy-GRA approach can significantly enhance AVC performance-yielding higher attenuation, lower energy consumption, and greater robustness-while remaining amenable to practical implementation in smart composite beam systems.

This study demonstrates that integrating fuzzy logic with grey relational analysis offers a powerful, mathematically rigorous framework for tuning active vibration control in smart composite beams, yielding significant improvements in vibration attenuation (up to 29.7 %), energy efficiency (up to 15.3 % savings), and robustness to both parameter uncertainty and environmental variations, while its statistical validation and real-time implementation prospects underscore its practical viability and broad applicability to advanced structural health-monitoring and precision engineering applications.

Author contributions: Conceptualization, Y.N. and N.R.; methodology, Y.N. and M.K.; software, M.K. and R.M.; validation, Y.N., M.K. and R.M.; formal analysis, Y.N.; investigation, Y.N., M.K. and A.K.S.; resources, N.R. and A.V.; data curation, R.M. and A.K.S.; writing-original draft preparation, Y.N.; writing-review and editing, Y.N., M.K., N.R., A.V., R.M. and A.K.S.; visualization, N.R. and M.K.; supervision, A.V. and Y.N.; project administration, Y.N.; funding acquisition, A.V. All authors have read and agreed to the published version of the manuscript.

Conflict of interest: The authors declare no conflict of interest.

References

1. Zhang S, Chen Z, Zhang X. Robust active vibration control of flexible smart beam by μ-synthesis. Journal of Sound and Vibration. 2025; 596: 118737. doi: 10.1016/j.jsv.2024.118737
2. Jirasek R, Schauer T, Bleicher A. Linear parameter-varying output-feedback for active vibration control of an elastic kinetic roof structure with experimental validation. Engineering Structures. 2024; 307: 117887. doi: 10.1016/j.engstruct.2024.117887
3. Hashemi A, Jang J, Hosseini-Hashemi S. Smart active vibration control system of a rotary structure using piezoelectric materials. Sensors. 2022; 22(15): 5691. doi: 10.3390/s22155691
4. Li C, Shen L, Shao J, et al. Simulation and experiment of active vibration control based on flexible piezoelectric mfc composed of pzt and pi layer. Polymers. 2023; 15(8): 1819. doi: 10.3390/polym15081819
5. Zadeh LA. Fuzzy sets. Information and Control. 1965; 8(3): 338–353. doi: 10.1016/S0019-9958(65)90241-X
6. Deng JL. Introduction to grey system theory. Journal of Grey System. 1989; 1(1): 1–24.
7. Crawley EF, De Luis J. Use of piezoelectric actuators as elements of intelligent structures. AIAA Journal. 1987; 25(10): 1373–1385. doi: 10.2514/3.9792
8. Soong TT, Spencer B. Active Structural Control: Theory and Practice. John Wiley & Sons; 2002.
9. Liu S, Lin Y. Grey Systems: Theory and Applications. Springer; 2010. doi: 10.1007/978-3-642-16158-2.

10. Lee CC. Fuzzy logic in control systems: fuzzy logic controller. I. IEEE Transactions on Systems, Man, and Cybernetics. 1990; 20(2): 404–418. doi: 10.1109/21.52551
11. Jang JSR. ANFIS: adaptive-network-based fuzzy inference system. IEEE Transactions on Systems, Man, and Cybernetics. 1993; 23(3): 665–685. doi: 10.1109/21.256541
12. Kennedy J, Eberhart R. Particle swarm optimization. In: Proceedings of the ICNN'95-International Conference on Neural Networks; 27 November–1 December 1995; Perth, Australia. IEEE; 1995. pp. 1942–1948. doi: 10.1109/ICNN.1995.488968
13. Yogeesh, N. Solving fuzzy nonlinear optimization problems using evolutionary algorithms. In: Advances on mathematical modeling and optimization with its applications. CRC Press; 2024.
14. Kuo Y, Yang T, Huang G-W. The use of grey relational analysis in solving multiple attribute decision-making problems. Computers & Industrial Engineering. 2008; 55(1): 80–93. doi: 10.1016/j.cie.2007.12.002
15. Timoshenko SP. On the correction for shear of the differential equation for transverse vibrations of prismatic bars. The London, Edinburgh, and Dublin Philosophical Magazine and Journal of Science. 1921; 41(245): 744–746. doi: 10.1080/14786442108636264
16. Reddy JN. An Introduction to the Finite Element Method, 3rd ed. McGraw-Hill; 2005.
17. Qiu ZC, Zhang XM, Wu HX, Zhang HH. Optimal placement and active vibration control for piezoelectric smart flexible cantilever plate. Journal of Sound and Vibration. 2007;301(3–5):521–543. doi: 10.1016/j.jsv.2006.10.018.
18. Hagood NW, Von Flotow A. Damping of structural vibrations with piezoelectric materials and passive electrical networks. Journal of Sound and Vibration. 1991; 146(2): 243–268. doi: 10.1016/0022-460X(91)90762-9
19. Yogeesh, N. Intuitionistic fuzzy hypergraphs and their operations. In: Applied Computer Vision and Soft Computing with Interpretable AI. Chapman & Hall/CRC; 2023.
20. Anderson BDO, Moore JB. Optimal Control: Linear Quadratic Methods. Prentice Hall; 1990.
21. Åström KJ, Murray RM. Feedback Systems: An Introduction for Scientists and Engineers. Princeton University Press; 2008.
22. Yogeesh N. Fuzzy Clustering for Classification of Metamaterial Properties: In: Advances in Wireless Technologies and Telecommunication. IGI Global; 2023. pp. 200–229. doi: 10.4018/978-1-6684-8287-2.ch009
23. Yogeesh N. Fuzzy Logic Modelling of Nonlinear Metamaterials: In: Advances in Wireless Technologies and Telecommunication. IGI Global; 2023. pp. 230–269. doi: 10.4018/978-1-6684-8287-2.ch010
24. Xu Q, Ruan X, Wei J. An iterative output feedback controller-design strategy for energy-to-peak structural vibration control. Journal of Asian Architecture and Building Engineering. 2024; 23(4): 1371–80. doi: 10.1080/13467581.2023.2270018
25. Tsao HSJ, Liu H. Optimal sequencing of test conditions in 2k factorial experimental design for run-size minimization. Computers & Industrial Engineering. 2008; 55(2): 450–64. doi: 10.1016/j.cie.2008.01.006